Fast Scattering Simulation Tool for Multi-Energy X-Ray Imaging

A. Sossin, J. Tabary, V. Rebuffel, J. M. Létang, N. Freud and L. Verger

***Abstract*–A combination of Monte Carlo (MC) and deterministic approaches was employed as a means of creating a simulation tool capable of providing energy resolved x-ray primary and scatter images within a reasonable time interval. Libraries of Sindbad, a previously developed x-ray simulation software, were used in the development. A cross-validation of the method against an analog MC (EGS4) simulation and a GATE simulation was performed. Results in terms of absorbed energy images obtained by the simulation tool proved to be in agreement with those generated by EGS4 and GATE with a global error of 9.28% and 5.76%, respectively. The difference in spectra, when compared to EGS4, was 4.21%–7.89%. Having the capability of being significantly faster than an analog MC approach, the hybrid method was able to generate a complete spectral scatter image within 1.5 hours using a single core 2.83 GHz CPU. Finally, a demonstration of the spectral capabilities of the developed tool is given by analyzing x-ray scatter in the energy domain.**

I. Introduction

THE development of radiographic systems and medical image processing techniques is often facilitated with the aid of computer simulation tools. An appropriate modeling of all the physics of the radiographic chain as well as a detailed description of its components is necessary to obtain x-ray images comparable to those acquired with a real system. Within the framework of this modeling scattered radiation plays an important part as it is known for introducing artifacts into the resulting images in the case of uncollimated geometry.

The x-ray simulation software Sindbad [1] is capable of modeling a realistic radiographic set-up. A combination of analytical and hybrid MC approaches is applied to compute both the primary and scattered contributions, respectively.

With the emergence of new energy discriminating photon counting semiconductor-based x-ray detectors [2], additional functionalities have been incorporated into Sindbad in order to produce energy resolved radiographic and tomographic x-ray images [3]. However, only primary radiation was concerned by this modification.

The purpose of this study is to demonstrate a recently developed Sindbad-based simulation tool with the ability to provide both energy-resolved primary and scatter x-ray images in a reasonable time.

Manuscript received November 7, 2014.

A. Sossin, J. Tabary, V. Rebuffel and L. Verger are with CEA-LETI MINATEC Grenoble, F-38054 Grenoble Cedex 09, France (e-mail: artur.sossin @cea.fr).

J. M. Létang and N. Freud are with CREATIS, INSA Lyon, 7 av. Jean Capelle, 69621 Villeurbanne Cedex, France (e-mail: jean.letang@insa-lyon.fr).

II. Simulation Tool

An energy resolved x-ray image can be represented by a 3D matrix (Fig. 1), where each point *(x, y)* contains a spectrum sampled at a certain rate (depending on the energetic resolution of the detector).

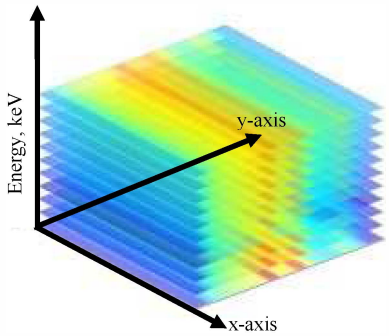

Fig. 1. Example energy resolved x-ray image.

When simulating x-ray scatter images, the introduction of energy information would significantly increase computational demand, if one were to use an analog MC simulation. In order to have accurately resolved x-ray spectra in each image point, a higher number of photons would need to be used in the simulation.

In order to provide reasonable computation times while not sacrificing accuracy, a Sindbad – Spectral Fixed Forced Detection (SFFD) simulation tool was designed. The SFFD scatter simulation approach is based on a combination of MC and deterministic calculations [4] with spatial sub-sampling of the detector.

Firstly, the MC part determines the set of scattering points $\{P_1, \ldots, P_{i-1}, P_i, P_{i+1}, \ldots, P_n\}$ in the object by tracking each particle from the emission point until being absorbed or exiting the boundaries of the simulation. Coordinates, propagation direction, incident photon energy, event type (Compton or Rayleigh) and event order are recorded for each interaction point P_i. Florescence is not handled as it begins to add a significant contribution only when a fair amount of high atomic number material is present in the object.

The second part of the method applies a deterministic calculation of the particle fractions $f_{ij}(E_i, E_{ij}^*)$ arriving from each scattering point P_i on a given node point N_j located on the detector:

$$f_{ij}\left(E_i, E_{ij}^*\right) = \frac{1}{\sigma_i\left(E_i\right)} \frac{d\sigma\left(\theta_{ij}, E_i\right)}{d\Omega} \exp\left(-\sum_q \mu^q\left(E_{ij}^*\right) r_{ij}^q \right) \Omega_{ij} \,, \quad (1)$$

978-1-4799-6097-2/14/$31.00 ©2014 IEEE

where $\sigma_t(E_i)$ is the total cross-section as a function of the incident photon energy E_i for scattering from P_i over 4π sr, $d\sigma(\theta_{ij},E_i)/d\Omega$ is the differential cross section, θ_{ij} is the scattering angle, $\mu^q(E_{ij}^*)$ is the linear attenuation coefficient of a given material q constituting the object, function of the scattered photon energy E_{ij}^*, r^q_{ij} is the path length traversed by the scattered particle fraction in the respective material and Ω_{ij} is the solid angle seen by the scattering source P_i on the node point N_j corresponding to a given detector pixel. Assuming a perfect detector, the scatter spectrum $S_j(E_{ij}^*)$ in each node point N_j is computed using the following expression:

$$S_j\left(E_{ij}^*\right)=\sum_i f_{ij}\left(E_i,E_{ij}^*\right), \qquad (2)$$

The final part of SFFD consists of determining the spectra for the entire detector by interpolating between the acquired samples N_j. Sub-sampling was implemented assuming that scattered radiation is spatially slowly varying distribution [5].

An illustrative summary of the presented approach can be observed in Fig. 2.

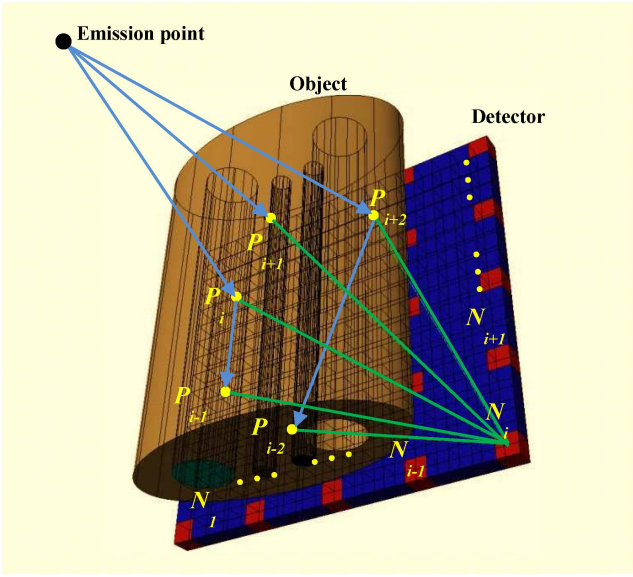

Fig. 2. Schematic reflecting different parts of the SFFD x-ray scatter simulation approach. The MC generated particles are shown interacting with the object and producing a set of scattering points of different order followed by a sum of particle fractions calculation in the direction of the given node.

III. Cross-Validation

To examine the accuracy of the developed tool in terms of x-ray scatter simulation performance (SFFD approach), a comparison was carried out with the aid of an analog MC (EGS4) [6] and another simulator – GATE [7]. One does not consider the validation of the primary x-ray image generation part of Sindbad-SFFD as it is completely based on the previous version of the software (Sindbad) and was validated in [3].

A. Simulation Parameters

A numerical simplified constructive solid geometry (CSG) thorax phantom in a radiographic geometry was used for cross-validating SFFD (Fig. 3). Global system parameters used for image generation for all 3 simulators were: a tube spectrum at 110 kVp and 1 mAs with 2.5 mm of Al filtration, a 512×512 pixel ideal detector (1 mm pitch). Additionally, for the SFFD, 5×10^6 initial photons and a 32×32 regular node grid followed by a trilinear interpolation between the node points were applied. EGS4 and GATE simulations were set up with 10^9 and 9.9×10^{10} initial photons, respectively. Furthermore, the EGS4 simulation was run 10 times to improve statistics and compute the standard deviation for the resulting images and spectra. EGS4 and SFFD simulations were run on a single core 2.83 GHz CPU while GATE was run on a single core 3.1 GHz CPU.

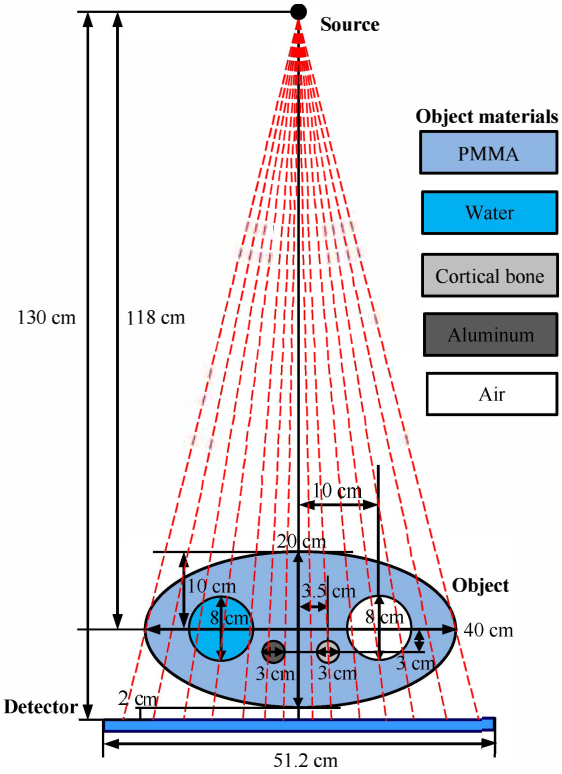

Fig. 3. An illustration of the numerical phantom and geometry used in the cross-validation (axial plane). The phantom is composed of an elliptical cylinder 50 cm in height with four cylindrical inserts of the same height.

B. Qualitative Analysis

Firstly, a primary x-ray image (i.e. without scatter) is generated to provide an idea of how the structures of the object in Fig. 3 are projected on the detector plane given the respective geometry (Fig. 4).

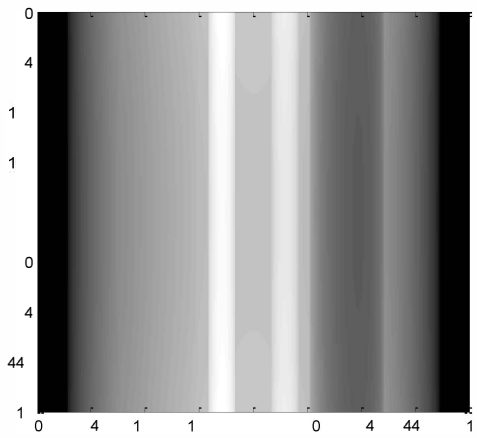

Fig. 4. Primary x-ray image. Note that the Al, bone and air inserts show high contrast with respect to the object base. The water insert is barely visible as its mass attenuation coefficient function is close to that of PMMA.

Absorbed energy scatter images were acquired with all three simulators (Fig. 5 and Fig. 6). EGS4 provided additional scatter spectra from 16×16 pixel image sub-zones, which were compared to equivalent spectra produced by SFFD (Fig. 7).

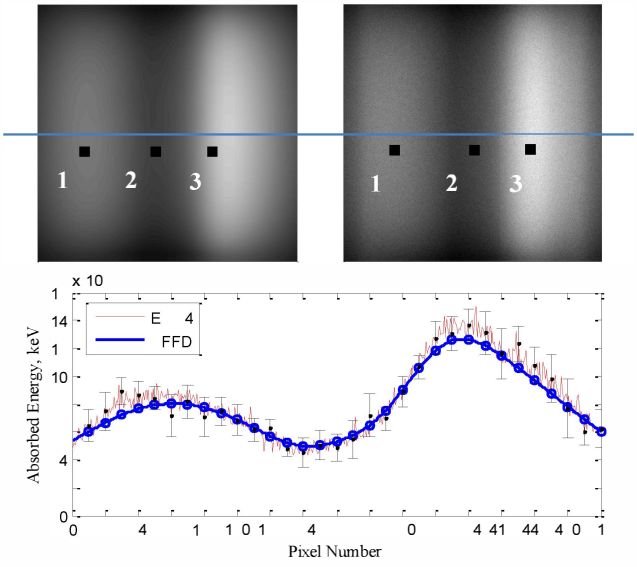

Fig. 5. Absorbed energy scatter images produced by SFFD (left) and EGS4 (right) with the corresponding central profiles (below). Note the marked sub-zones in the images for further spectral comparison. SFFD node points are marked with circles. Standard deviation (σ) of the EGS4 simulation is represented by black error bars.

Examination of Fig. 5 comparing SFFD and EGS4 reveals a similar spatial pattern of the total absorbed scattered radiation energy with the SFFD providing a less noisy spatial distribution due to the deterministic part of the algorithm. Otherwise, Sindbad-SFFD has the option of adding the photon noise after the SFFD simulation. Central profiles show a high degree of agreement between the two simulators with the SFFD remaining largely within the 2σ interval of the EGS4. The zones where the criterion is not satisfied for one or several points are: pixel #32-96 (near the left object border), pixel #352-416 (air insert) and pixel #416-480 (near the right object border). In these zones one notes a sub-estimation with respect to EGS4.

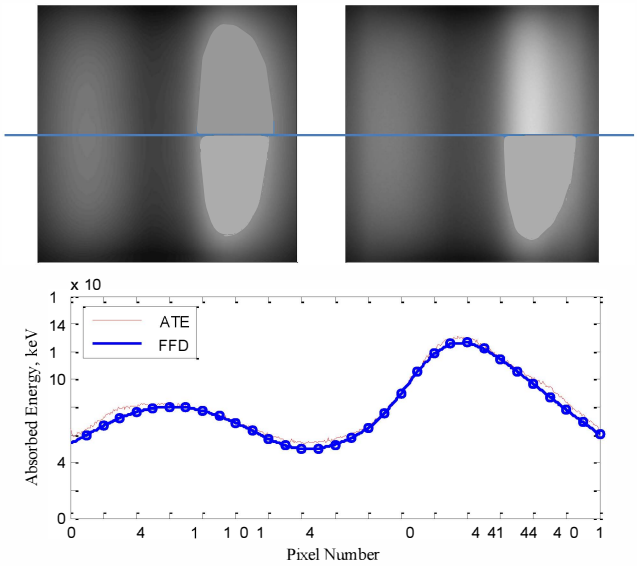

Fig. 6. Absorbed energy scatter images produced by SFFD (left) and GATE (right) with the corresponding central profiles (below). SFFD node points are marked with circles. The profile of GATE is not accompanied by error bars corresponding to the standard deviation as it is in the order of 10^3 and would not be visible at the current scale.

Fig. 6 shows a satisfying agreement in terms of absorbed energy images when comparing the designed tool with GATE. Because of the higher initial photon count used in the simulation by the former (compared to EGS4), both images (GATE and SFFD) display an equal level of smoothness, which was not the case in Fig. 5. From the central profiles one immediately notices the same sub-estimation provided by the SFFD with respect to GATE. However, it is not only the parts corresponding to the object borders and air insert that are concerned, but also the part containing the highly attenuating inserts (Al and cortical bone).

Overall, the performance of SFFD in terms of absorbed energy scatter images is acceptable. The inconsistencies in different image regions are possibly due to: an insufficient number of scattering points, a large distance between the grid points or the method of interpolation used.

Further support of the agreement between SFFD and EGS4 is seen from the sub-zone scatter spectra (Fig. 7) with the developed tool being well within the error margins of EGS4. Additionally, spectral shapes exhibit a high degree of similarity. Finally, an examination of peaks in the spectra reveals a sub-estimation by the SFFD. This is due to trilinear interpolation. As noted before, a spectral x-ray image is a 3D matrix (Fig. 1). It is important, however, that the nature of dimensions is not equivalent: two spatial dimensions with one energetic dimension. Applying a trilinear interpolation causes smoothing in 3 dimensions. While the scatter signal is slowly varying spatially, it does not exhibit the same behavior in the energy domain (characteristic peak). Thus, a smoothing in the

peaks of the spectra outside the node grid can be generated. This could not only explain the peak inconsistencies visible in Fig. 7 but also the differences observed previously in Fig. 5 and Fig. 6.

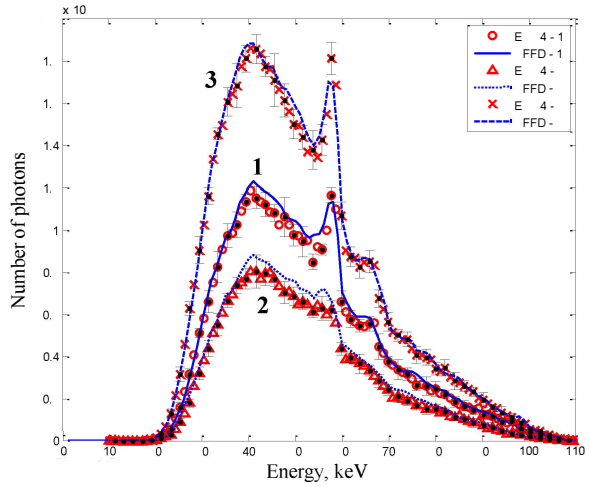

Fig. 7. Scatter spectra taken from the image sub-zones marked in Fig. 5. Energy channel width is equal to 1 keV.

C. *Quantitative Analysis*

In order to quantify the differences in absorbed energy scatter images, a metric known as the normalized root-mean-square error (NRMSE) was used:

$$NRMSE_I = \frac{1}{I_{ref}(x,y)}\sqrt{\frac{\sum_{x,y}\left[I_{ref}(x,y)-I_{SFFD}(x,y)\right]^2}{N_p}}, \qquad (3)$$

where I_{ref} and I_{SFFD} are the absorbed energy images generated by EGS4 or GATE and SFFD, respectively. N_p is the number of pixels in the image.

For the generated sub-zone spectra a similar metric (4) is applied in the energy interval 20-100 keV. This eliminates the contribution of channels with a low number of photons.

$$NRMSE_S = \frac{1}{S_{ref}(E)}\sqrt{\frac{\sum_{x,y}\left[S_{ref}(E)-S_{SFFD}(E)\right]^2}{N_E}} \qquad (4)$$

In (3) S_{ref} and S_{SFFD} are the spectra generated by EGS4 and SFFD, respectively. N_p is the number of channels in the spectrum.

The $NRMSE_I$, when comparing the designed tool with EGS4 and GATE, was 9.28% and 5.76%, respectively. A better global agreement with GATE was anticipated, since the image is much less noisy than the one produced by the analog MC simulator. It is also more indicative of the actual global SFFD performance in terms of absorbed energy images.

For the three spectra presented in Fig. 7 the $NRMSE_I$ was 4.21% (#1), 6.03% (#2), 7.89% (#3), respectively. The growth of error according to the overall signal level can be traced to the deviations in the peak area that grow accordingly.

In terms of computation time SFFD, EGS4 and GATE used 1.5, 15 and 17 hours, respectively. It is worth also noting that the grouping of image pixels into sub-zones was chosen to provide sufficient photon statistics for the spectra in the case of EGS4. For the current case, the developed tool was already around 10 times faster than EGS4 with SFFD providing a complete 512×512 pixel spectral x-ray scatter image while EGS4 provided a 32×32 sub-zone equivalent. For the analog MC approach to provide a full spectral image while maintaining the current statistics, an increase of simulation time by another factor of ~16^2 can be expected.

IV. Analysis of Scattered Radiation

To demonstrate the spectral capabilities of Sindbad-SFFD, a brief analysis of scattered radiation in the energy domain is provided.

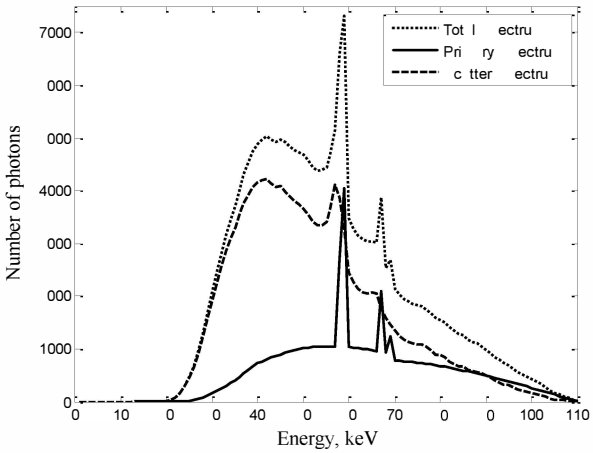

Fig. 8. Total, scatter and primary spectra obtained from the central pixel taken from the sub-zone #1 of the SFFD scatter image (Fig. 5). The number of MC shower photons was increased to 5×10^7 to provide better energetic resolution. The scatter signal is ~117% higher than that of the primary (total absorbed energy).

Scattered radiation is known to induce undesired modifications in the recorded x-ray signal. From Fig. 8 one can immediately notice the increase in overall signal level when scatter is taken into account. This is especially visible in the low-energy interval. Finally, the shape of the total spectrum changes and it becomes closer to that of the scatter rather than the primary.

One now decomposes the scatter spectrum of Fig. 8 into single and multiple scatter for further examination (Fig. 9).

Fig. 9 shows that, for the current case, multiple scatter signal is about 2 times higher than the single scatter signal. Additionally, if compared, primary spectrum (Fig. 8) and single scatter spectrum are relatively close in shape and level while multiple scatter displays a much larger difference having a smooth distribution shifted to the low energy region with an almost complete absence of characteristic peaks.

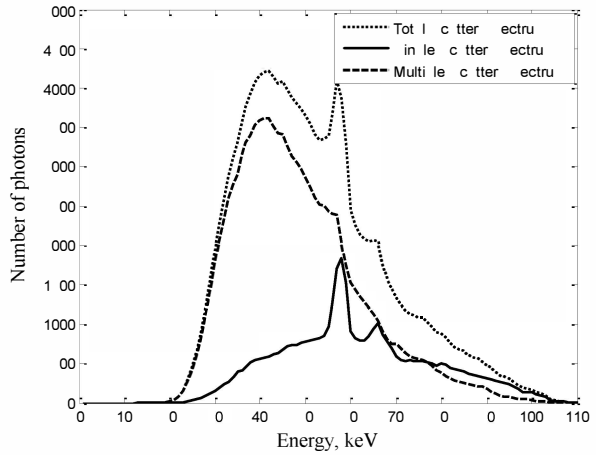

Fig. 9. Scatter spectrum from Fig. 8 separated into single and multiple (interactions of order >2) components.

V. CONCLUSIONS AND PERSPECTIVES

Current cross-validation results depict a satisfying performance for the developed software both in terms of absorbed energy and spectral x-ray scatter images. The trends of sub-estimation observed in the absorbed energy images will require further examination by varying the algorithm parameters (grid, interpolation, photon number) and, possibly, using a simpler object. A cross-validation of the spectral part of SFFD scatter simulation approach, using GATE, is to be carried out. The Sindbad-SFFD x-ray simulation tool is able to model complex anthropomorphic numerical phantoms and provides the possibility to incorporate a detector response model in the simulations. With the aid of these capabilities an experimental validation of the tool is also planned to be performed.

The presented simulation tool has the potential of becoming a valuable instrument for studies of scattered radiation in energy resolved x-ray imaging. Furthermore, SFFD will be used to study scatter correction methods for multi-energy x-ray imaging.

REFERENCES

[1] J. Tabary, R. Guillemaud, F. Mathy, A. Glière, and P. Hugonnard, "Combination of high resolution analytically computed uncollided flux images with low resolution Monte Carlo computed scattered flux images," IEEE Trans. Nucl. Sci., vol. 51, no. 1, pp. 212–217, 2004, Oct. 2005.

[2] A. Brambilla, P. Ouvrier-Buffet, J. Rinkel, G. Gonon, C. Boudou, and L. Verger, "CdTe Linear Pixel X-Ray Detector With Enhanced Spectrometric Performance for High Flux X-Ray Imaging," IEEE Trans. Nucl. Sci., vol. 59, no. 4, pp. 1552–1558, Aug. 2012.

[3] V. Rebuffel, J. Tabary, P. Hugonnard, E. Popa, A. Brambilla, G. Montemont, and L. Verger, "New functionalities of SINDBAD simulation software for spectral X-ray imaging using counting detectors with energy discrimination," in NSS/MIC, 2012 IEEE, 2012, pp. 2550–2554.

[4] N. Freud, J.-M. Letang, and D. Babot, "A hybrid approach to Simulate X-ray imaging techniques, combining Monte Carlo and deterministic algorithms," IEEE Trans. Nucl. Sci., vol. 52, no. 5, pp. 1329–1334, Oct. 2005.

[5] J. H. Siewerdsen, M. J. Daly, B. Bakhtiar, D. J. Moseley, S. Richard, H. Keller, and D. A. Jaffray, "A simple, direct method for x-ray scatter estimation and correction in digital radiography and cone-beam CT," Med. Phys. vol. 33, no. 1, pp. 187–197, Jan. 2006.

[6] J.C. Satterthwaite, "EGSNova : An adaptation of EGS in C/C++," Nov. 1998. [Online]. Available at : http://rcwww.kek.jp/research/egs/epub/aap/js3nov98.html

[7] S. Jan, D. Benoit, E. Becheva, T. Carlier, F. Cassol, P. Descourt, T. Frisson, L. Grevillot, L. Guigues, L. Maigne, C. Morel, Y. Perrot, N. Rehfeld, D. Sarrut, D. R. Schaart, S. Stute, U. Pietrzyk, D. Visvikis, N. Zahra, and I. Buvat, "GATE V6: a major enhancement of the GATE simulation platform enabling modelling of CT and radiotherapy," Phys. Med. Biol., vol. 56, no. 4, pp. 881–901, Feb. 2011.